Biofilm Neutrophils Interactions Under Hypoxia: A Mathematical Modeling Study

Andreas C. Aristotelous[1,2]

Department of Mathematics
Buchtel College of Arts and Sciences
The University of Akron
Akron, Ohio, 44325-4002, USA

Abstract

Neutrophils are important to the defense of the host against bacterial infection. Pathogens and the immune system cells create via respiration, a hypoxic environment in infected regions. Hypoxic conditions affect both the neutrophil's ability to eradicate the infection and also change the behavior of the bacterial-pathogens by eliciting the production of various virulence factors, the creation of bacterial biofilm and the initialization of anaerobic metabolism. In this work interactions of bacterial biofilm and neutrophils are studied in a domain where oxygen is diffusing into the environment and is being consumed by biofilm. Within a hypoxic environment, bacteria grow anaerobically and secrete higher levels of toxin that diffuses and lyses neutrophils. A mathematical model explicitly representing the biofilm volume fraction, oxygen, and diffusive virulence factors (toxin) as well as killing of bacteria by neutrophils is developed and studied first in 1D and then in 2D. Stability analysis and numerical simulations showing the effects of oxygen and toxin concentration on neutrophil-bacteria interactions are presented to identify different possible scenarios that can lead to elimination of the infection or its persistence as a chronic infection. Specifically, when bacteria are allowed to utilize anaerobic breathing and or to produce toxin, their fitness is enhanced against neutrophils attacks. A possible insight on how

[1]The author was partially supported by NSF-DMS 1720226
[2]Corresponding author: aaristotelous@uakron.edu

virulent bacterial colonies can synergistically resist neutrophils and survive is presented.

Keywords: `Virulence Factors, Toxin, Anaerobic Metabolism, Stability Analysis, Numerical Simulations`

1. Introduction

Bacterial biofilms are clusters of bacteria that stick to surfaces, multiply, and are encased in a matrix of extracellular polymers produced by either the microorganism or the defensive mechanisms of the host [1, 2]. Biofilms are very difficult to treat, because they are resistant to antimicrobials and also shield themselves from external threats and impede the ability of host immune cells to eradicate them. More than 60% of bacterial infections in humans are thought to be biofilm-related [3].

The most common immune cells in fighting infections are neutrophils which utilize phagocytosis, degranulation, and formation of neutrophil extracellular traps (NETs) to fight bacterial pathogens [4]. Microorganisms, on the other hand, utilize various strategies to evade clearance by neutrophils [5]. Strategies, include anaerobic metabolism, which allows the microorganisms to continue growing and being metabolically active in the absence of oxygen [6], production of various toxins that lyse the immune cells [7] and physical exclusion of immune cells by the biofilm matrix. The mechanisms and dynamics of the interaction between neutrophil and biofilm are complex and multifactorial.

There is a significant interest in the study of the interaction between bacteria and immune cells like neutrophils under hypoxia, and the understanding of the underlying mechanisms could lead to the creation of novel therapies. We are motivated and guided by recent experimental and review work [8, 9, 10, 11, 12, 13]. There is a lot of uncertainty in the mechanisms governing the interaction of the immune cells and biofilm under hypoxia, with some even contradictory experimental results [8]. The effects of hypoxia in this setting are poorly understood (see [8]-figure 3A). We strive to provide some insight to the

complicated interactions using a modeling approach to investigate the potential contributions of hypoxia [14] to the biofilm defense against neutrophil attack. For this purpose we construct a spatial fully continuum phenomenological model that describes the evolution of biofilm volume fraction as a result of biofilm growth and elimination by neutrophils. We lump all neutrophil's actions against biofilm into the term "phagocytosis".

For our mathematical model we make the following modeling assumptions. We assume that biofilm density (or volume fraction) is growing, and microbial biofilm has little or no motility or diffusion. Also we assume that there is an abundance of neutrophils distributed everywhere in our domain, which we only model their effects without explicitly model their population density, for simplicity. In our model we allow for biofilm growth by both aerobic and anaerobic metabolism. Oxygen diffuses into the domain and is being absorbed by the bacterial biofilm by a reaction diffusion mechanism. Biofilm is assumed to grow logistically with aerobic growth that follows Monod kinetics [15]. In the case where aerobic growth is relatively small due to low oxygen concentration, first order kinetics simulating anaerobic growth are employed. We incorporate into our model the adverse effect that hypoxia has on neutrophil phagocytosis [8], by limiting appropriately the effectiveness of neutrophil phagocytosis on biofilm, whenever oxygen level is low. We are also accounting for the fact that neutrophil bacterial phagocytosis is diminished when biofilms form dense structures, that is, when biomass volume fraction is high enough [5, 16, 17]. Our model incorporates some virulence factors that microbes employ to inhibit neutrophils such as the production of toxin [7, 5, 8, 9, 10, 11, 12, 13]. Specifically, we lump together all diffusing virulence factors in one variable which we refer to as "toxin". Toxin production increases as oxygen levels decrease [18, 19, 20].

We analyze our model in one and two dimensions and provide insights as to how the local oxygen concentration within the infection site, serves as a trigger for biofilm virulent factors. This in combination with bacterial concentration and spatial distribution/location, relative to the oxygen source within the infection site, are paramount for the ability of neutrophils to succesfully deal with

the infection.

The paper is organized as follows. In section 2, we introduce a mathematical model and then analyze its behavior first by performing a local stability analysis in a nonspatial setting. This gives us a fist insight to the dynamics of the full spatial model and various parameter regimes. In section 3 we proceed to analyze the full model via simulation in one spatial dimension, identifying the model components contributing to elimination or persistence of the biofilm infection. Subsequently, in section 4 we simulate in two spatial dimensions and we propose a scenario where virulent bacterial colonies survive synergistically. In section 5 we describe the numerical methods we use and finally in section 6 we finish with concluding remarks.

2. Model Description

We consider a square infection region where blood vessels constantly transport oxygen on one of its outer sides ("top"), and the oxygen diffuses into the interior of the infected region. At the top, the blood vessels also sweep away any diffusing toxin that reaches the top boundary away from the infected region.

We remark here that we consider microbes to be distributed inside a background matrix where new biofilm growth results in increased local biomass density rather than expansion of the structure. This is different from many biofilm models, like in [21], where growth-driven pressure causes biofilm expansion and deformation. Also we note that for the oxygen and toxin we suppose that the domain is thin enough so that the time-scale for reaction-diffusion processes to equilibrate is significantly shorter than the growth time scale. That is, we assume quasi-equilibrium and for this reason we neglect the time derivative when writing the reaction diffusion equations describing the evolution of toxin and oxygen. This is a common assumption in many biofilm models [22].

We introduce the biofilm volume fraction $0 \leq \theta(x, z, t) \leq 1$ and let $c(x, z, t) \geq 0$, $w(x, z, t) \geq 0$ be the oxygen and biofilm-produced toxin concentration respectively, α is the phagocytosis coefficient, r the biofilm growth rate coefficient, D_c

and D_w are the diffusion coefficients of oxygen and toxin respectively which are assumed constant. Also d is the toxin degradation rate and $q(c)$ the toxin production which is heightened by lower c concentration [18, 19, 20], that is, $q(0) = 1$ and $q(c) \to 0$ as c increases, so a possible choice is $q(c) = 1 - c/(c + N_c)$.

With decreasing oxygen, the production of toxins w increases, further decreasing the phagocytosis efficiency of neutrophils [18] and this is modeled by $T(w) = 1 - w/(w + N_w)$. Phagocytosis by neutrophils becomes more efficient with increasing c [23] and less efficient with decreasing c [24, 5], i.e., $p(c)$ is chosen to be increasing such that $0 < p(0) = p_0 << 1$, $0 < p(0) \leq p(c) \leq 1$ and $p(c) \to 1$ as c is increasing. Phagocytosis becomes less efficient with increasing θ [5, 16, 17] and we assume reduced susceptibility of biofilm to neutrophil phagocytosis when the local cell density exceeds a threshold [25], i.e., $f(\theta)$ is chosen such that $f(0) = 1$ and $f(1) = \epsilon > 0$, where ϵ 'small'. In absence of more evidence a logical choice for these functions is

$$p(c) = \frac{(1 - p_0)c}{(c + N)} + p_0 \quad \text{and} \quad f(\theta) = \begin{cases} 1, & \text{if } 0 \leq \theta < 0.5K_\theta \\ \epsilon, & \text{if } 0.5K_\theta \leq \theta \ , \end{cases} \tag{1}$$

where N is a nutrient half-saturation rate regarding phagocytosis. In simulations we smooth, f, as follows,

$$f(\theta) = 0.5(1 - \epsilon)\left(1 - \tanh\left(\frac{\theta - 0.5}{0.005}\right)\right) + \epsilon$$

and choose $\epsilon = 0.1$.

We consider a two dimensional domain $\Omega := \mathbb{R} \times [0, L]$ with Dirichlet, $c(x, L) = u_L$, $w(x, L) = 0$, and no-flux, $\frac{dc}{dn}(x, 0) = 0$, $\frac{dw}{dn}(x, 0) = 0$, boundary conditions. The boundary condition $w(x, L) = 0$ is chosen to simulate the scenario that the toxin is being swept away by blood flow on the top boundary. The biofilm initial condition is $\theta(x, z, 0) = \theta_0(x, z)$.

Considering all of the above we write the following system of equations

describing our model

$$\theta_t = Yr\hat{g}(c)h(\theta) - \alpha T(w)p(c)\theta f(\theta) := F(c,w,\theta)\,, \tag{2}$$

$$0 = D_c \triangle c - r\theta g(c), \tag{3}$$

$$0 = D_w \triangle w + r_w q(c)\theta - dw. \tag{4}$$

Here $h(\theta) = \theta(1-\theta/K_\theta)$ where $K_\theta = 1$ is used to model the biofilm limited growth, this choice prevents volume fraction from increasing beyond $\theta = 1$, oxygen uptake follows Monod kinetics, $g(c) = \left(\frac{c}{c+K}\right)$ and K is the substrate absorption half-saturation rate. We introduce anaerobic metabolism/growth in (2) by setting $\hat{g}(c)$ equal to a fixed value $g_{anaerobic}$ whenever $g(c)$ is smaller than $g_{anaerobic} > 0$,

$$\hat{g}(c) = \max(g(c),\ g_{anaerobic})\,, \tag{5}$$

where $g_{anaerobic} << 1$.

The focus of our model is the interaction between biofilm and the immune response due to neutrophils under hypoxia, without aiming to model in detail the complicated biofilm composition and biofilm-flow interaction as done in [26, 27]. Using a relatively simpler biofilm representation, allows us to analyze first via stability analysis and then by numerical simulations, the complicated interactions between pathogen(biofilm) and immune response (neutrophils) and better understand their dynamical interplay. The important modeling work done in [28] studies the emergence of a persister type due to toxin, omitting any immune response or anaerobic metabolism. The model proposed herein, is a significant evolution of the models in [29, 30], where biofilm was interacting only with diffusing oxygen. In [14] the authors incorporated neutrophil and biofilm only to study oxygen depletion in a wound, but did not incorporate biofilm killing by neutrophils nor virulent factors like toxins or anaerobic metabolism and their various interactions, which in our model created a more dynamic environment between the two.

To the best of our knowledge, this is the only work that presents a mathematical model that combines all the following: neutrophil (mediated by biofilm

structure and oxygen amount) killing of biofilm, where biofilm is also allowed to perform anaerobic metabolism and to produce diffusing toxin that can lyse the neutrophil cells, in a dynamic environment all acting together. Our modeling framework could be extended and adapted to multiple biological scenarios.

2.1. Dimensional Analysis

In our model dimensional values for diffusion are measured in mm^2/min, length L is in mm and time is in minutes (min). Oxygen diffusion $D_c \sim 0.05\ mm^2/min$ and oxygen reaction $r \sim 25\ min^{-1}$ values are within the ranges reported in [31] and [14] respectively. The $\sqrt{D/r}$ ratio important for active layer for oxygen penetration, is the same used in [29]. For the value of the combined toxin diffusion $D_w = 0.006\ mm^2/min$, we use the fact that toxin is a larger molecule than oxygen, thus we choose an order of magnitude value consistent with [31]-example 1. To observe the interdependency between the various model parameters, for the system we rewrite it in the following non-dimensional form although such process is not unique and the original system could be exactly in its original form with all its parameters scaled and non-dimensional. The system (2)-(4) can be rewritten as:

$$\begin{aligned} \bar{\theta}_\tau &= Y \max\left(\frac{\bar{c}}{\bar{c}+0.5}, g_{anaerobic}\right)\bar{\theta}(1-\bar{\theta}) \\ &\quad -\lambda\frac{\bar{\theta}}{\bar{w}+0.5}\left[\frac{(1-p_0)\bar{c}}{(\bar{c}+\mu)}+p_0\right]\hat{f}(\bar{\theta}), \qquad (6) \\ 0 &= \bar{\triangle}\bar{c} - \beta\bar{\theta}\frac{\bar{c}}{\bar{c}+0.5}, \qquad (7) \\ 0 &= \bar{\triangle}\bar{w} + \delta\frac{\bar{\theta}}{\bar{c}+\gamma} - \eta\bar{w}. \qquad (8) \end{aligned}$$

where

$$\hat{f}(\bar{\theta}) = \begin{cases} 1, & \text{if } 0 \le \bar{\theta} < 0.5 \\ \epsilon, & \text{if } 0.5 \le \bar{\theta}\ . \end{cases}$$

The new variables and functions are $\bar{\theta} = \theta/K_\theta$, $\bar{c} = c/(2K)$, $\bar{w} = w/(2N_w)$, the independent variables are $\bar{x} = x/L$, $\bar{z} = z/L$ and $\tau = rt$. The non-dimensionalized parameters are $\lambda = \alpha/(2r)$, $\mu = N/(2K)$, $\beta = rK_\theta L^2/(D_c 2K)$,

$\gamma = N_c/(2K)$, $\delta = r_w \gamma K_\theta L^2/(D_w 2N_w)$ and $\eta = dL^2/D_w$. From this analysis, we see that important parameters regulating the dynamics are Y, $g_{anaerobic}$, λ, β and δ. Later in simulations we test our system for different values of $g_{anaerobic}$ and δ the latter corresponding to the original r_w parameter, which are the ones regulating anaerobic metabolism and toxin production respectively. We choose to keep all other parameters to some fixed value.

2.2. Nonspatial Stability Analysis

Now we assume a non-spatial setting and consider (6) as a simple ordinary differential equation (ODE). In this way we strive to obtain some helpful insight about the dynamics of our system. This will allow us to have some theoretical understanding when interpreting the model's simulation results since at any given point in the domain the biofilm there would follow the ODE local dynamics. We drop the "bars" and "hats" for simplicity of notation from the dimensionless model (6)-(8), and assume fix position in the domain or a spatially independent setting, then we have for the biomass,

$$\theta_\tau = Y g(c) h(\theta(\tau)) - \lambda T(w) p(c) \theta f(\theta(\tau)) \,. \tag{9}$$

Set $\bar{r} := Y g(c) > 0$ and $a := \lambda T(w) p(c) > 0$. So we have a two parameter space. Then for θ-equilibria we have

$$\bar{r}\theta(1-\theta) = a\theta f(\theta) = \begin{cases} a\theta, & \text{if } 0 \le \theta < 0.5 \\ \epsilon a \theta, & \text{if } 0.5 \le \theta \le 1 \,. \end{cases} \tag{10}$$

Equilibria are θ-values satisfying the above equation or precisely where the growth curve $\bar{r}\theta(1-\theta)$ and phagocytosis curve $a\theta f(\theta)$ intersect or where $\bar{r}\theta(1-\theta) - a\theta f(\theta)$ changes sign (see Fig. 1). The importance of equilibrium values θ^* in our case is that if they are asymptotically stable then biofilm volume fraction values "close" to the equilibrium value will tend towards the equilibrium as time increases and if they are unstable will tend away form it. So this knowledge gives us some rudimentary insight into the evolution of biofilm assuming we know the equilibria values *a priori*.

For all the different values of the bifurcation parameters $a, \bar{r}$ the curves "intersect" in different points corresponding to different equilibrium values. By increasing gradually the value of the phagocytosis parameter α keeping $\bar{r}$ fixed, we generate all the possible different regimes which are the different panels shown in figure 1. In each panel an equilibrium value θ^*, measured on the horizontal axis, is asymptotically stable if the growth curve (red) is above the phagocytosis curve (blue) for $\theta < \theta^*$ and if it is also below for $\theta > \theta^*$.

By observing the panels of figure 1 corresponding to equilibria for various values of the bifurcation parameters $a, \bar{r}$, we can see that the only case that we have multiple equilibria and $\theta^* \equiv 0$ is an asymptotically stable equilibrium is when $a > 0.5\bar{r}$ and specifically when $a \geq \bar{r}$. We are interested in the case where $\theta^* \equiv 0$ is asymptotically stable since this means that the biofilm is able to be cleared by the neutrophils and this is more biologically relevant. When $0.5\bar{r} < a < \bar{r}$ then $\theta^* \equiv 0$ is unstable and as $a \to \bar{r}$ we have that a positive asymptotically stable equilibrium collides with the zero unstable equilibrium (see Fig. 1c, 1d) and they "exchange" stability, thus we have a transcritical bifurcation and $\theta^* \equiv 0$ becomes asymptoticaly stable.

The case $\bar{r} \leq a < 0.5\bar{r}/\epsilon$ is of interest to us since we observe the emergence of an Allee effect, meaning there are three equilibria, with the middle, $\theta_2^* \equiv 0.5$ unstable and the other two $\theta_1^* \equiv 0$ and $0.5 < \theta_3^* < 1$ asymptotically stable. It is interesting to study when this behavior also emerges locally by using the fully spatial nonlinear model (6)-(8), since in this case if biofilm volume fraction is between the first and the middle equilibrium then the infection gets cleared and if it is above the middle then it persists. Finally, the case $a \geq 0.5\bar{r}/\epsilon$ corresponds to one asymptotically stable trivial (zero) equilibrium and thus the infection is aways cleared.

3. Simulation Results in 1D

In this section we perform various simulations in order to understand the mechanics of our system and also shed some light on the interplay between biofilm

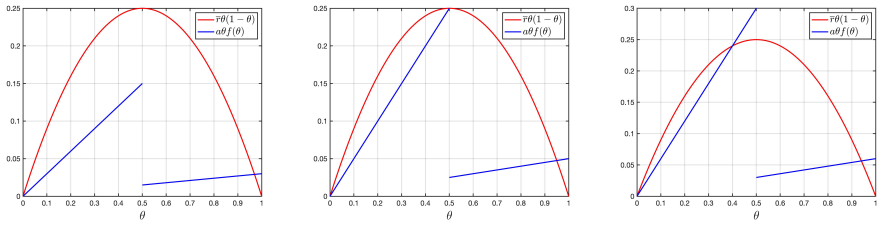

(a) $a < 0.5\bar{r}$ (b) $a = 0.5\bar{r}$ (c) $0.5\bar{r} < a < \bar{r}$

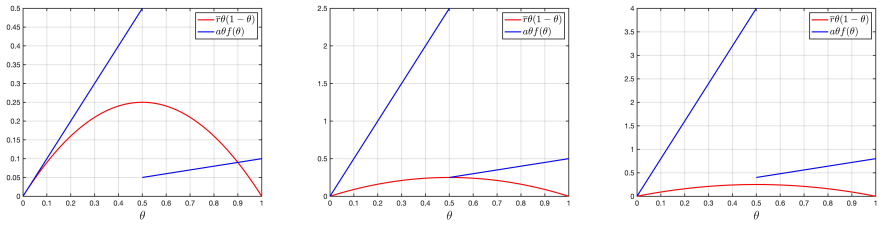

(d) $a = \bar{r}$ (e) $a = 0.5\bar{r}/\epsilon$ (f) $a > 0.5\bar{r}/\epsilon$

Figure 1: Nonspatial stability analysis cases. Intersection and jumps of the biofilm growth, $\bar{r}\theta(1-\theta)$, and phagocytosis, $a\theta f(\theta)$, curves lead to equilibria. Panel 1a corresponds to a stable growth towards the carrying capacity asymptotically stable equilibrium, panel 1b is the critical case when transitioning to more than one nonzero equilibria. Panel 1c is for $0.5\bar{r} < a < \bar{r}$ (corresponding to four equilibria) and panel 1d depicts the critical case when $a = \bar{r}$ (corresponding to three equilibria–Allee Effect). Panel 1e is the critical case that leads to 1f corresponding global biofilm extinction. Figure parameters: $\bar{r} = 1$, $\epsilon = 0.1$.

and neutrophils in certain scenarios. We concentrate first on 1D spatial models to understand the mechanism of our system, incrementally adding features like anaerobic metabolism, toxin and finally combining them together. The dynamics are guided by non-dimensional parameter ratios thus scaled base parameters are chosen (see figure 2) so at the oxygen diffusing boundary, $z = L = 1$, our model follows the nonspatial dynamics of figure 1d (i.e., $\theta^* \equiv 0$ asymptotically stable). This is the biologically relevant scenario, since it allows even at the oxygen diffusive boundary, the possibility of clearance of the infection when biofilm volume fraction is sufficiently low.

3.1. Density-Dependent Protection

We investigate the 1D scenario closely related to the nonspatial scenario in figure 1d. We have for the specific region, $z_c \leq z \leq 1$ close to the oxygen diffusive boundary (at $z = 1$), that the system has three equilibrium solutions $u_1^*(z) \equiv 0$, $u_2^*(z) \equiv 0.5K_\theta$ and $0.5K_\theta < u_3^*(z) < K_\theta$ (we take $K_\theta = 1$). The values, $u_3^*(z)$, of the largest equilibrium, vary according to the oxygen and toxin level at $z > z_c$. We choose first to remove the effects of toxin and anaerobic metabolism and focus on just the interaction between biofilm and neutrophil effects in the presence of the diffusing oxygen.

In figure 2 we use initial uniform biofilm conditions to demonstrate the three equilibria close enough to the oxygen diffusive boundary. In the first row we have initial biofilm profile $\theta_0 = 0.45$, and we observe that the biofilm is gradually decreasing to zero, with different rates at each domain point, as time progresses. Observe (see figure 2b) that the biofilm follows two different dynamics. It is cleared faster in the part of the domain closer to the boundary (which follows figure 1d) while at the same time more gradually is being eliminated further away (following figure 1f). This is because the dynamics closer to the boundary are faster due to the presence of oxygen which helps the action of neutrophils [23, 24, 5]. So for our parameter selection this illustrates that the $\theta^* \equiv 0$ is an asymptotically stable equilibrium and at the same time the $\theta^* \equiv 0.5$ is unstable for any initial biofilm $\theta_0 < 0.5$. In the same figure, we also plot the

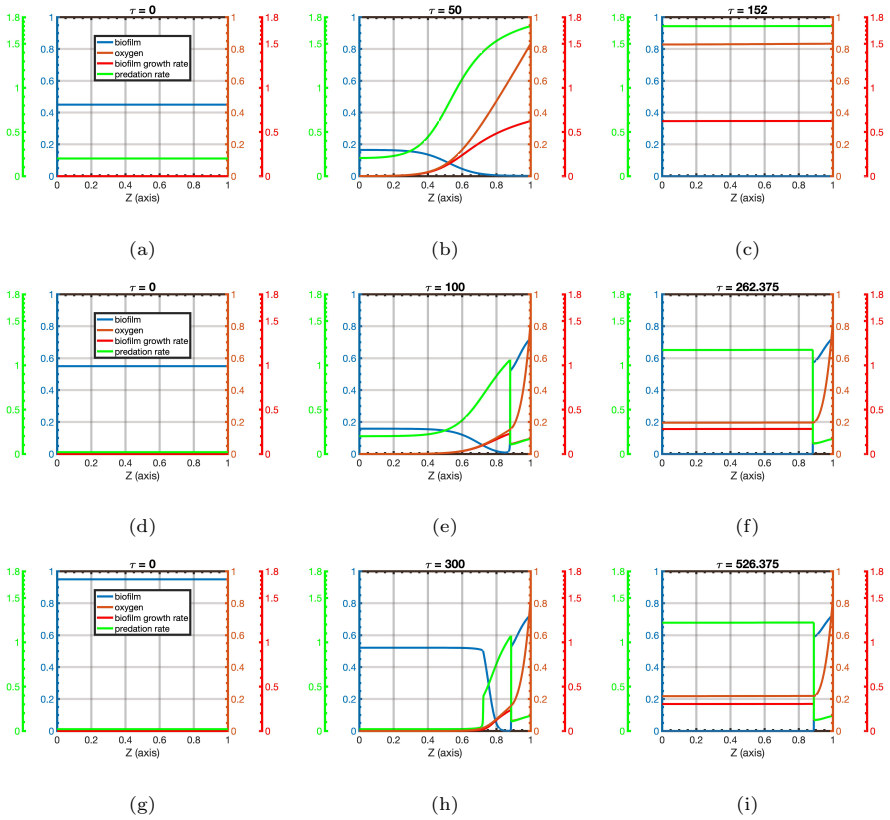

Figure 2: Local Allee Effect–Uniform biofilm initial condition $\theta_0 = 0.45$(first row), $\theta_0 = 0.55$(second row), and $\theta_0 = 0.95$(third row). Initial time, Intermediate time and "steady state" snapshots of biofilm θ (blue) for each case. Other functions are oxygen c (brown), biofilm death rate or neutrophil action rate $\lambda T(w)p(c)f(\theta)$ (green) and also biofilm growth rate $Y\hat{g}(c)(1-\theta)$ (red). $t = \tau/r$. Base parameters: $\epsilon = 0.1$, $p_0 = 0.1$, $Y = 1.0$, $r = 25$, $K = 0.6$, $K_\theta = 1$, $L = 1$, $\alpha = 50$, $N = 0.2$, $D_c = 0.05$, $D_w = 0.006$, $N_w = 0.5$, $N_c = 0.7$ and $d = 0.003$, corresponding to the dimensionless ratios $\epsilon = 0.1$, $p_0 = 0.1$, $Y = 1.0$, $\lambda = 1$, $\mu = 1/6$, $\beta = 416.67$, $\gamma = 0.583$ and $\eta = 0.5$.

oxygen level, neutrophil phagocytosis rate and biofilm growth rate. Observing the various panels corresponding to the same time instance we can better track the interaction between oxygen, biofilm and neutrophils. Equilibrium is reached when the growth rate is equal to the phagocytosis rate or when the biofilm is eliminated. This outcome corresponds to the cure or resolution of a biofilm infection.

For the same parameter choice and a uniform initial biofilm, $\theta_0 = 0.55$ in figure 2-row 2 we observe that only a part of the biofilm closer to the boundary is "repelled" away from $\theta^* = 0.5$, and converges to the third equilibrium, $0.5 < u_3^*(z)$, mimicking the prediction of figure 1d, for $z > z_c \approx 0.87$, locally close to the diffusing boundary. The sharp drop of the biofilm at $z \approx 0.87$ is due to the nature of the neutrophil phagocytosis term $\lambda p(c) f(\theta)$ that peeks at that part of the domain. For $z < z_c$ the biofilm decreases eventually to zero since oxygen is slowly penetrating and this favors the neutrophils on the interface for our parameter choice, also where oxygen is zero neutrophil phagocytosis is very small and equal to ϵ but not zero and since biofilm growth is zero for zero oxygen we have that eventually neutrophils win there. This outcome corresponds to the persistence of the biofilm infection.

Finally in figure 2–row 3 we use initial uniform biofilm, $\theta_0 = 0.95$ and we observe that the biofilm eventually returns to a profile, that resembles the last biofilm panel in figure 2-row 2, further corroborating the fact that for at least $z > z_c \approx 0.87$ we have an asymptotically stable third equilibrium and the emergence of an "Allee Effect" locally, in that region of the domain. The biofilm for $z < z_c$ decreases again to zero. This tells us that for $z < z_c$ we are on another stability regime with only one equilibrium (as in figure 1f), where the phagocytosis function is always greater than the growth function for that part of the domain.

The local Allee effect in theory guarantees the survival of the biofilm closer to the oxygen source with this set of parameters, as long as the biofilm has high enough volume fraction (e.g., $\theta > 0.5$) as required by the parameter regime. This tells us that any virulent factor, that will help the biofilm closer to the diffusive

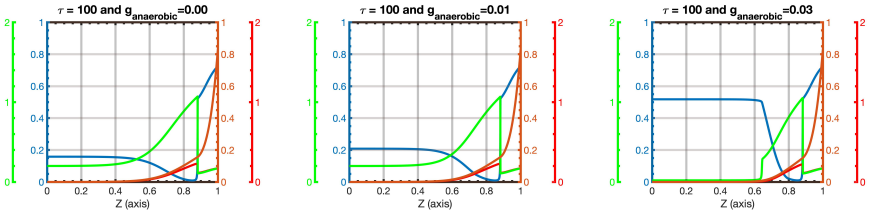

(a) (b) (c)

Figure 3: Low Anaerobic Metabolism. Uniform biofilm initial condition $\theta = 0.55$. Simulation snapshots for fixed transient time, $\tau = 100$, of biofilm θ with anaerobic metabolism using $g_{anaerobic} = 0.0$, 0.01 and 0.03. Biofilm eventually dies off for $z < z_c$ relatively quickly in all cases. E.g. for $g_{anaerobic} = 0.01$ steady state, see figure 6a. Biofilm θ (blue), oxygen c (brown), biofilm death rate or neutrophil action rate $\lambda T(w)p(c)f(\theta)$ (green) and biofilm growth rate $Y\hat{g}(c)(1-\theta)$ (red). $t = \tau/r$.

boundary to increase its volume fraction above the threshold $\theta_c = 0.5$ [25], will result in biofilm survival, even if the initial biofilm was below that threshold (cf. Fig. 5). This outcome again corresponds to the persistence of a chronic biofilm infection.

3.2. Effects of Biofilm's Anaerobic Metabolism

To investigate the effects of anaerobic metabolism we introduce a constant parameter that accounts for anaerobic growth as described in (5). We choose the same base parameters as in figure 2 with initial uniform biofilm concentration $\theta = 0.55$, and vary the values of $g_{anaerobic}$. In figure 3 for some fixed transient time, we observe that for nonzero $g_{anaerobic}$ the biofilm infection for $z < z_c$ is higher as the anaerobic metabolism parameter increases. It is worth noting that for all cases in figure 3 the biofilm eventually goes to zero for $z < z_c$ since the oxygen penetrates slowly while the biofilm is eliminated close to z_c and thus allows the neutrophils to become more effective progressively deeper inside the domain until the infection is eradicated, for $z < z_c$ (for a longer simulation corresponding to $g_{anaerobic} = 0.01$, cf. Fig. 6a).

However, for sufficiently large value, e.g. $g_{anaerobic} = 0.3$, the infection persists indefinitely in all regions of the domain and reaches a steady state

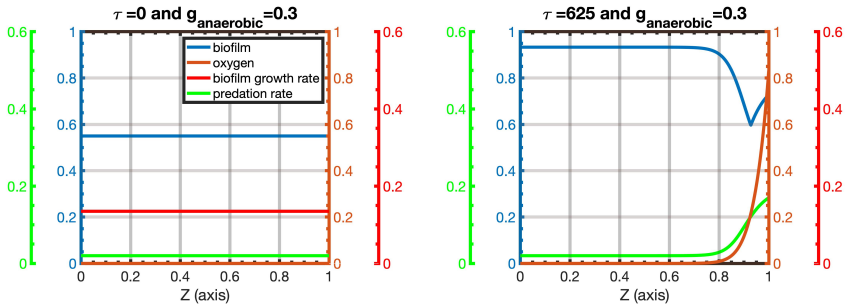

(a) (b)

Figure 4: High Anaerobic Metabolism. Biofilm survival. Panel 4a: uniform biofilm initial condition $\theta = 0.55$. Panel 4b: steady state of biofilm θ with anaerobic $g_{anaerobic} = 0.3$. Biofilm θ (blue), oxygen c (brown), biofilm death rate or neutrophil action rate $\lambda T(w)p(c)f(\theta)$ (green) and biofilm growth rate $Y\hat{g}(c)(1-\theta)$ (red). $t = \tau/r$.

(cf. Fig. 4). This high relative ratio choice between maximum anaerobic and aerobic growth, is similar to the relative growth ratio, ~ 0.26, between growth in well oxygenated vs highly hypoxic setting described in table 1, of [32] for *Pseudomonas Aeruginosa*. Other bacteria like *Pseudomonas Fluorescens* have even higher relative growth ratios ~ 0.5, (see table 1 in [33]). For some bacteria though, this anaerobic value might be quite high, hence, in subsequent tests in section 3.4 we explore lower amounts of toxin and anaerobic employed together.

We note that the action of anaerobic growth happens only in parts of the domain sufficiently away form the diffusive boundary ($z < z_c$), where oxygen is low enough and thus its effect is sharp due to the localized nature of the anaerobic function in (5). In terms of a clinical infection outcome, the capacity for anaerobic respiration under hypoxia, enhances biofilm formation [20] and this is in agreement with our model prediction.

3.3. Effects of Biofilm's Diffusive Virulence Factors

In this section we explore the effects of diffusing virulence factors. One example is the production of cytotoxin by the biofilm that lyses the neutrophils [5, 8, 9, 10, 11, 12, 13]. We set the anaerobic metabolism to zero and vary the rate,

δ, of toxin production in (8). Since the virulence factors diffuse at various concentrations in all parts of the domain even in parts of the domain where they were not originally produced, these factors effectively help the biofilm to survive or to persist longer before eradication, in that part of the domain. In figure 5

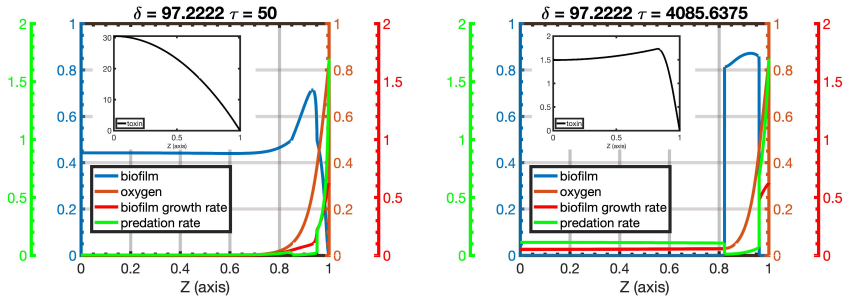

(a) (b)

Figure 5: Highly Virulent. Diffusive Virulence Factors. Panel 5a: uniform IC profile $\theta = 0.45$. Panel 5b: steady state of biofilm θ. Same parameter as figure 2, with the addition of $\delta \approx 97$. Biofilm θ (blue), oxygen c (brown), biofilm death rate or neutrophil action rate $\lambda T(w)p(c)f(\theta)$ (green) and biofilm growth rate $Y\hat{g}(c)(1-\theta)$ (red). $t = \tau/r$. Toxin is depicted in the inset figure.

we observe the survival of biofilm that is highly virulent in contrast with the biofilm simulation that uses the same parameters, but has no virulence factors, (see figure 2-row 1), which eventually dies off everywhere. The biofilm in figure 5 secretes at the early stages high enough toxin (see figure 5b) to decrease the phagocytosis rate "nearly" to zero in the majority of the domain and to have the phagocytosis rate lower than the growth rate close enough to the diffusive boundary. This is due to the fact that at this stage of the simulation the biofilm that is away from the diffusive boundary is highly hypoxic and maintains its original mass, thus secreting more toxin [9, 10]. Where the growth rate is higher than the phagocytosis rate in proximity to the diffusive boundary, the biofilm grows above the "threshold" 0.5 value with the help of toxin that diffuses from all the parts of the domain, hence at least at that part its survival is guaranteed because of the dynamics, even if the biofilm eventually very slowly is being

eradicated at parts of the domain away from the oxygen diffusive boundary. We note here that the eradication of the biofilm in those parts, is due to the fact that early on an active layer blocks oxygen from reaching the biofilm away from the diffusive boundary and since the phagocytosis term is never zero even while oxygen is zero — unlike the biofilm growth term which is zero when there is no oxygen — this gives to the neutrophils a competitive advantage in absence of anaerobic metabolism. We can theorize here, that for this setting, anaerobic metabolism is also needed to help the survival of biofilm in the part of the domain where oxygen is zero. Even if in the last profile oxygen is penetrating in low concentrations the parts away from the boundary, it was not enough to save the biofilm there from the neutrophils, in a hypoxic environment with only toxin production and no anaerobic growth.

Since we use zero boundary condition for the toxin on the oxygen diffusive boundary our nonspatial stability analysis says that with this parameter choice, at that part of the domain we expect the biofilm to locally die off, and indeed this is happening in that small region neighboring the top boundary, where the action of toxin is zero or very negligible, the biofilm follows the dynamics observed in figure 2-row 1. This insight from the stability analysis helps us evaluate the validity of our simulation results and is very useful.

3.4. Combined Biofilm Virulence Factors

For this section we combine the effects of anaerobic growth and production of toxin. We fix a toxin production level and anaerobic value such that each individual virulence factor (e.g., toxin, anaerobic metabolism) alone is unable to guarantee biofilm survival (cf. Fig. 6a and 6b) for $z < z_c$. In figure 6c we observe that the combined effect of bacterial-biofilm anaerobic metabolism and toxin production results in the survival of biofilm for $z < z_c$, where there, the absence of one of the two contributing factors causes the biofilm to die off. In figure 6c, toxin is nonzero everywhere except on the top boundary where it decreases monotonically to zero. Toxin has an effect on the biofilm profile even in the domain part where $z > z_c$ where oxygen is high enough unlike anaerobic

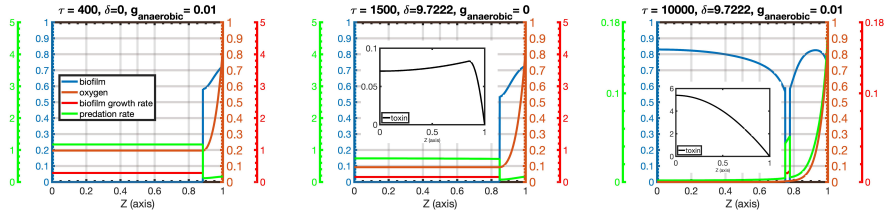

(a) (b) (c)

Figure 6: Combined anaerobic and toxin effects result in survival of biofilm–Uniform biofilm initial condition $\theta = 0.55$. Base parameters as in figure 2. Steady States: Panel 6a depicts biofilm density and has toxin production turned off with anaerobic turned on and set to $g_{anaerobic} = 0.01$, the panel 6b shows biofilm density with anaerobic off but toxin production rate turned on set to $\delta \approx 9.7$, the panel 6c also shows biofilm density having both anaerobic metabolism and toxin production turned on set to $g_{anaerobic} = 0.01$ and $\delta \approx 9.7$. Biofilm θ (blue), oxygen c (brown), biofilm death rate or neutrophil action rate $\lambda T(w)p(c)f(\theta)$ (green) and biofilm growth rate $Y\hat{g}(c)(1-\theta)$ (red). $t = \tau/r$. Toxin is depicted in the inset figure.

metabolism which kicks in only at approximately $z < z_c$ where oxygen is low enough.

So we observe that a relatively small amount of anaerobic metabolism in combination with a comparatively small rate of toxin production acting in synergy guarantee the longer survival and growth of biofilm in parts of the domain where each one of these factors alone is unable to do that. This mimics closer the natural biofilm processes where under hypoxia a combination of various anaerobic metabolism and toxin production is utilized to achieve biofilm survival and growth [19, 20].

The dip in figure 6c can be explained, because our model predicts different dynamic behaviors on the left and right of z_c. The dip starts forming right on the threshold of the competing dynamical behaviors. The dip observed, starts forming earlier on the simulation, where there is enough oxygen at z_c, for the neutrophils to overwhelm the biofilm there. Since the biofilm, gets completely eliminated at that point the dip remains, because in our model the biofilm grows only in height, and not laterally. Although we could observe such features in experimental biofilm profiles e.g., [34]-figure 1c, we are not aware of

an existing experimental result that illustrates specifically that such a dip is due to neutrophil action.

3.4.1. Biofilm Initial Distribution Effect

To test the effect of how the distribution of biofilm in the 1D domain might effect its growth and survival we compare the scenario in figure 6 with a scenario that has the same total initial biofilm volume fraction but uniformly distributed only on the half domain, the one closer to the diffusive boundary, $z > 0.45$, (see figure 7). For this test we observe that the setup that has the initial

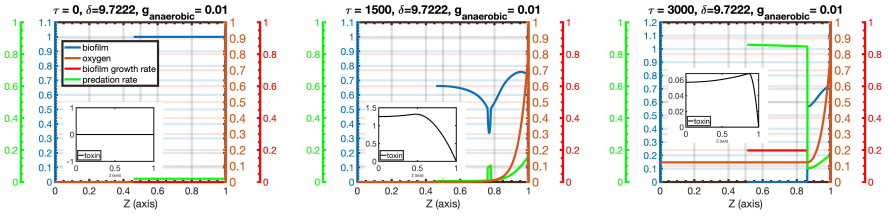

(a) (b) (c)

Figure 7: Combined anaerobic and toxin effects simulations with a concentrated initial biofilm distribution–Parameters as in figure 6c. First panel depicts the initial condition for biofilm with $\theta_0 = 1$ on $[0.45, 1]$. Second and third panels: intermediate time snapshot and steady state snapshot corresponding to ICs. Biofilm θ (blue), oxygen c (brown), biofilm death rate or neutrophil action rate $\lambda T(w)p(c)f(\theta)$ (green) and biofilm growth rate $Y\hat{g}(c)(1-\theta)$ (red). $t = \tau/r$. Toxin is depicted in the inset figure.

biofilm as in figure 6c i.e., uniformly distributed on the entire domain, survives in contrast to the biofilm corresponding to the initial biofilm distribution on the half domain, which eventually gets cleared by the neutrophils, for $z < z_c$, (see figure 7). By looking figures 7a and 7b we observe that the dynamics close to the boundary $z > z_c \approx 0.8$, quickly pull down a large part of the concentrated biofilm initial condition to the third asymptotically stable equilibrium, thus lowering a significant part of the biofilm concentration, effectively reducing the production of adequate toxin required for its survival in the region where $z < z_c$. This in combination with the higher oxygen concentration present due to longer active layer because of lower biofilm volume fraction, further diminishes

the toxin production there, and the result is that everything eventually with volume fraction $\theta < 0.5$ is cleared by neutrophils following similar dynamics as in figure 2-row 1. This is different from the spread profile example in figure 6c where more biofilm is located away from the diffusive boundary and oxygen is unable to penetrate there, thus larger portion of the biofilm can produce higher toxin levels contributing to longer survival and growth except from a very small extinction region where the neutrophils managed to "win".

We also observe that in both simulations (figure 6c and figure 7) the part of the biofilm, $z > z_c$ (z_c different in each of the two scenarios) survives and is on steady state following the dynamics we showed before in figures 2 second and third row, hence its partial survival as long as its initial volume fraction is greater than 0.5 is guaranteed with this choice of base parameters. We remark that the presence of toxin just adds to the value of the steady state biofilm at the part close to the diffusing boundary, by pushing it slightly higher than a scenario with no toxin.

The test also tells us that for example, if the case corresponding to figure 2-row 1 would have had the entire initial biofilm stacked in the half of the domain, i.e., $\theta_0 = 2 \times 0.45 = 0.9 > 0.5$, closer to the diffusion boundary $z > 0.5$, then at least the part of it corresponding to $z > z_c$ (for some z_c according to the chosen parameters), will survive, regardless of toxin or anaerobic effects, primarily due to the dynamics we described in figure 2-row 2,3.

4. Two Dimensional Biofilm

In this section using the same base parameters, we perform simulations to better illustrate the interaction between biofilm and neutrophils in two spatial dimensions (2D), by considering isolated colonies. In a previous work [29] we have demonstrated that a dense enough cluster of colonies behaves essentially as one with respect to diffusion, which is covered by the previous 1D discussion.

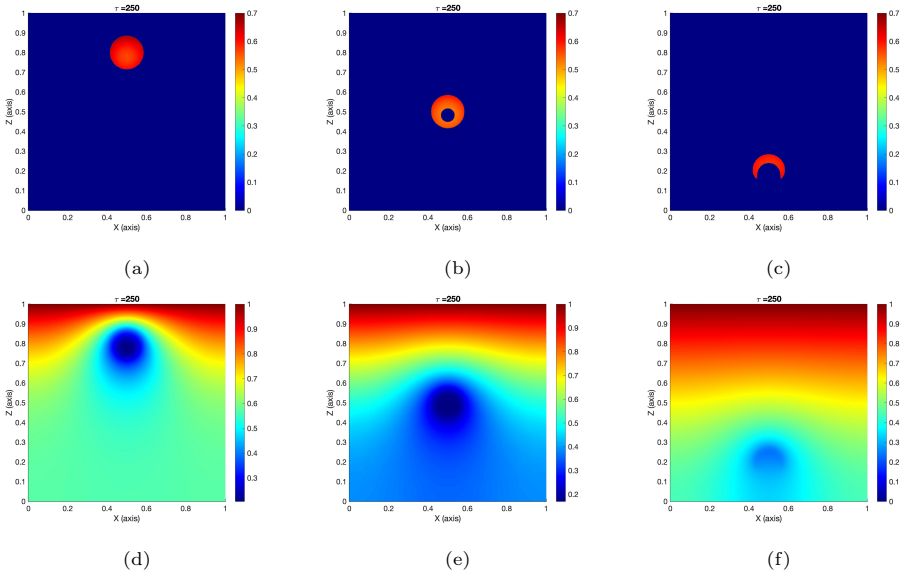

Figure 8: Single isolated 2D colony – Base parameters with anaerobic growth and toxin production both turned off. Initial condition colony is positioned successively at $x = 0.5$ and $z = 0.2, 0.5, 0.8$ with initial radius ≈ 0.1 and initial height 0.55. Oxygen diffuses at $z = 1$. Panels depict steady state profiles for each colony position. Second row depicts the corresponding oxygen profiles.

4.1. Minimum Height for Survival

Here we turn off the anaerobic growth and toxin production and examine the height of an isolated colony of radius ≈ 0.1 that guarantees its survival. We have – like in 1D – reached to the conclusion that in presence of sufficient oxygen, anything with height > 0.5 survives and anything with height < 0.5 gets cleared by the neutrophils for our previous choice of base parameters, in absence of anaerobic and toxin production. This also tells us that a very little amount of biofilm mass if it is stacked together is able to survive, which means the structure of biofilm matters for its survival [5, 16, 17], in contrast to being spread at heights < 0.5 which it dies, as shown in 1D.

To illustrate the importance of 2D, in figure 8 we position a single isolated colony of radius ≈ 0.1 and height 0.55, at three different positions, away from the oxygen diffusing boundary and we observe that although a part of the biomass is

surviving as expected, in each case, local features intrinsic to 2D are observed. On the panel 8a when the colony is positioned close enough to the diffusive boundary we observe that it survives and grows higher in the front part which is closer to the oxygen boundary. Sufficient oxygen is penetrating the colony but also diffuses from the colony sides so it reaches around it to the back side in sufficient amount so no part of it gets completely cleared. On the panel 8b we observe that not enough oxygen penetrated the interior of the colony resulting in the clearance of its "center core" slightly towards the backside, by the neutrophils. In the panel 8c we have that not only the interior gets cleared but also the entire part of the colony that is away from the diffusing oxygen front is also cleared.

This local behavior can be explained by looking to figure 2 rows 2 and 3 where in the transient panels the oxygen is low away from the boundary helping the neutrophils to push the biofilm lower than 0.5 there, resulting in the clearance of the biofilm, in absence of any virulence factors (or anaerobic breathing) of course. In the panel 8c after the formation of the crescent the oxygen (panel 8f) eventually has more room to diffuse and thus the surviving biofilm reaches little higher than the steady state height of the middle colony, due to slightly higher oxygen concentration there.

The understanding of the local behavior is useful since it highlights the specific parts of the colony that are hypoxic, where anaerobic metabolism and higher toxin production will be present when such features are turned on.

Finally we note that the radius of the colony affects the formation of the local features in relation to the distance form the oxygen diffusive boundary. For example a colony with higher radius is expected to exhibit the crescent like behavior when is closer to the boundary than a smaller radius one. An "infinite" radius colony is the simulation corresponding to the uniform initial biofilm profiles in 1D figure 2.

4.2. Virulent Colonies Survive in Synergy

In this section we position two colonies of radius (≈ 0.1) at $x = 0.5$ with one colony on the bottom ($z = 0.2$) at height 0.3 and the other colony on the top ($z = 0.7$) at height 0.45 (see figure 9 first row). We keep the same base parameters and turn on the anaerobic to $g_{anaerobic} = 0.3$ and the toxin production rate to $\delta \approx 97$. Also we include in this test a tiny biofilm diffusion ($D_b = 10^{-5}$) to allow for the biofilm colony to expand very slowly radially making the simulation more realistic. Both colonies at their respective locations in absence of the other get cleared by the neutrophils with the current parameters.

In figure 9 we observe the evolution of the two virulent colonies positioned together, working in synergy eventually resulting in their survival. Specifically the top colony while is being cleared by neutrophils "blocks" oxygen long enough and allows the bottom colony to grow in a hypoxic environment by utilizing anaerobic metabolism while producing higher levels of diffusing virulent factors (toxin) (see figure 9 second row). The bottom colony is growing in a sense protected by the top colony, which is attracting the bulk of the phagocytosis due to higher amounts of oxygen there and is continuously dying, to the point that is almost completely eradicated (see figure 9 third row).

After the bottom colony anaerobically grows high enough, it produces a sufficient amount of diffusing toxin that is able to arrest the phagocytosis of the top colony by neutrophils (especially on the side away from the oxygen diffusing boundary–the back side) and help it to start regrowing (see figure 9 fourth row). The top colony regrows more towards its back side because is more hypoxic there, since on its front with higher oxygen concentration there, neutrophils still "win" as long as the height is < 0.5 according to the dynamics we studied. Both colonies grow and their hypoxic parts increase in height with a very slight increase in radius allowing more toxin to be generated from their hypoxic regions and this feedback mechanism allows them to survive.

Any part of the top colony that has sufficient oxygen on it, is guaranteed to survive forever after its height reaches > 0.5 according to our dynamics and what we showed in figure 8 and the discussion therein, since anaerobic and toxin

has an additive effect on its fitness. This, results in more oxygen blockage with the rest of the colony parts growing using anaerobic and taking advantage of the reduced biofilm phagocytosis due to biofilm structure (height > 0.5) and also increased levels of toxin (coming from the top and bottom colonies via diffusion) (see figure 9 last row). The bottom colony is now protected fully by the top one and both together "feed" each other and survive in synergy.

An important observation made in designing the test is that the spatial arrangement of the two, colonies is vital to their synergistic survival under the described mechanism. One colony needs to be "close enough" above the other and directly in the path of diffusing oxygen in order for the synergistic survival mechanism to be effective and viable to the persistence of the infection. Otherwise, colonies spatial arrangement that position the two far apart or the top such that is not not directly in the diffusing oxygen result in infection elimination, with the current choice of our non-dimensional parameters.

In figure 9 all the features of our model are in action providing a possible explanation how multiple colonies could "work" together to fight off the host immune system by protecting each other. Synergistic interactions between bacterial colonies have been observed in other circumstances, for example when under antibiotic stress [35]. For this reason the feedback mechanism our model predicts might be a plausible explanation why infection overcomes the immune response in hypoxic conditions via colony synergy.

5. Numerical Solution

The equations used in our work are nonlinear and do not have analytical solutions. One of the important difficulties we want to address is that the biofilm colony profiles exhibit "near" vertical interfaces effectively making the solutions discontinuous at some parts, due to the competing dynamics in different parts of the domain. This makes it challenging to correctly numerically resolve them (see for example figures 8, and 2). For this reason, specialized high order and efficient numerical methods are required.

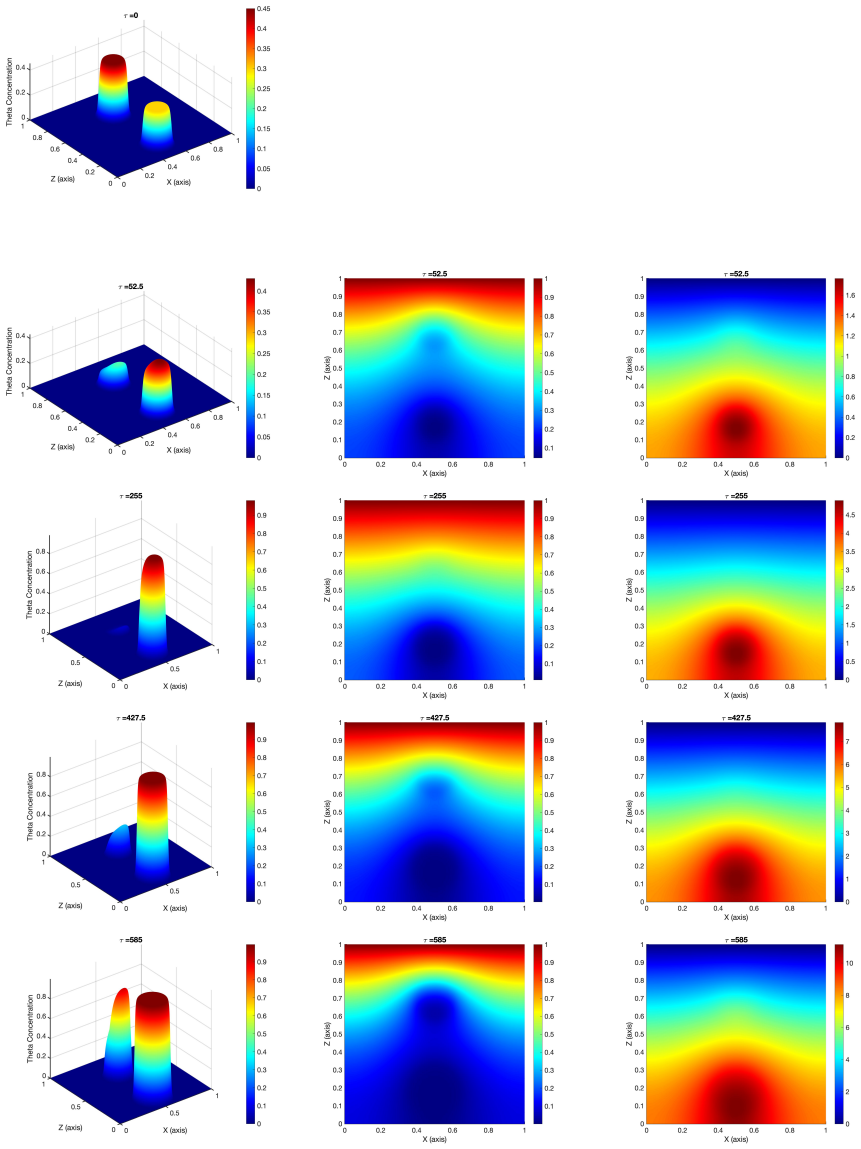

Figure 9: Two virulent colonies survive in synergy – Base parameters with anaerobic and toxin both turned on with $g_{anaerobic} = 0.3$ and $\delta \approx 97$. A very small amount of biofilm diffusion $D_b = 10^{-5}$ is added. Initial condition colonies are positioned at $x = 0.5$ and $z = 0.2, 0.7$ with initial radius 0.1 and initial height 0.3 for the bottom ($z = 0.2$) colony and 0.45 for the top ($z = 0.7$) one. First column depicts biofilm evolution. Second and third columns depict the corresponding oxygen and toxin profiles.

Consequently, we employ high-order mesh adaptive (h-adaptive) discontinuous Galerkin (DG) finite-element (FE) numerical schemes. Since finite elements generate a variational formulation of (2) – (4), the biofilm interface, can be handled using high-order numerical quadratures in conjunction with compatible meshes and mesh adaptivity. The adaptive algorithms and marking strategy follow the work done in [36, 37, 38]. High-order solution approximations can be obtained by using higher degree basis functions. Another attractive feature of the DG method is the ease with which it accounts for various types of boundary conditions by incorporating them into the weak formulation. A comprehensive review of DG methods for the spatial discretization of elliptic and other type of PDEs can be found in [39, 40, 41]. In our model's 2D numerical implementation we require periodic boundary conditions on the left and right parts of the boundary. The periodic boundary conditions are *implemented weakly* extending the ideas proposed in [42] for the Poisson equation. The method in [42] was presented on a uniform mesh and requires the existence of the same number of edges in the corresponding periodic boundaries. It suggests the creation of a map between matching periodic edges, $e_i,\ e_j \in \mathcal{E}^B$, defined as periodic pairs e_p, that is, $e_p := \{e_i, e_j\}$, where $e_i \subseteq \{x = 0\} \times [0, L]$ and $e_j \subseteq \{x = P\} \times [0, L]$,

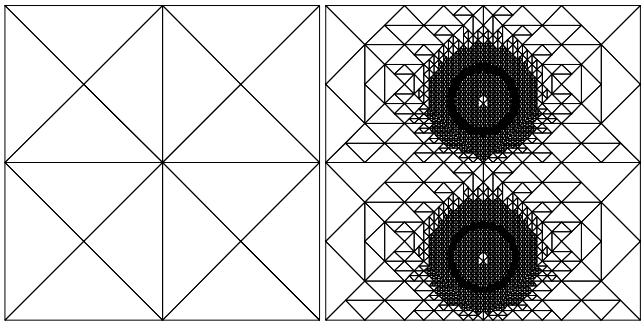

(a) (b)

Figure 10: Left: Initial (level 0) mesh used in all 2D computations, right: an instance of the evolving adaptive mesh (by refinement and coarsening) using quadrisection, supporting one hanging node per elemental edge and preserving the periodic edge map, used in the computations for figure 9.

(P is the length of the periodic domain) and $\mathcal{E}^p$ is the set of all periodic pairs. Essentially, a periodic pair is treated as a single interior edge and the corresponding extra terms are introduced in the bilinear forms. When dealing with adaptive meshes there is an additional level of complexity which we had to address in order to correctly maintain the periodic map due to the fact that refined periodic edges may create an imbalance to the number of edges on each periodic boundary (see figure 10). This was achieved by following the work done in [43, 30]. We note that the implementation of DG finite elements under the context of adaptive mesh refinement and coarsening (de-refinement) with periodic boundary conditions and multilevel solvers, is highly non trivial.

We now briefly describe the specific numerical method utilized to solve the governing equations in this study. For the time-stepping, the well-known theta-method is employed – the choice of $\Theta = 0.5$ corresponds to the Crank-Nicolson method which provides in theory second-order accuracy in time. We decouple the equations using a time relaxation on θ present in (11), (12) and thus they can be solved sequentially. We observed that this technique helped the stability of the numerical scheme. We arrive at the following fully discrete scheme for the system (2) – (4): Find $(\theta_h^n, w_h^n, c_h^n) \in V_h^q$ such that,

$$
\begin{aligned}
D_c\mathcal{B}_h(c_h^n, \chi) &= -(\theta_h^{n-1} g(c_h^n), \chi) + \mathrm{BT}_c^{Dirichlet}, && (11)\\
D_w\mathcal{B}_h(w_h^n, \chi) &= (r_w q(c_h^n)\theta_h^{n-1} - d w_h^n, \chi) + \mathrm{BT}_w^{Dirichlet}, && (12)\\
\left(\frac{\theta_h^n - \theta_h^{n-1}}{Dt}, \chi\right) &= \Theta\left(F(c_h^n, w_h^n, \theta_h^n), \chi\right) \\
&\quad +(1-\Theta)\left(F(c_h^n, w_h^n, \theta_h^{n-1}), \chi\right), && (13)
\end{aligned}
$$

where $\chi \in V_h^q$ is a DG basis function and V_h^q is the DG finite dimensional space [39] consisting of piecewise polynomial elements of degree, q. The usual L^2-inner product is denoted by $(\cdot,\cdot)$ and $\mathcal{B}_h^n(\cdot,\cdot)$ is the symmetric interior penalty DG bilinear form corresponding to the Laplacian operator in variational form with the prescribed BCs [42, 43, 30] and BT^D are boundary terms due to non-homogeneous Dirichlet BC. The qth-order DG basis polynomials, e.g. $q \in \{1, 2, 3, 4\}$, provide accuracy that is $O(h^{q+1})$ for the L^2-norm of the spatial error

at each time step, with h being the mesh discretization parameter.

In this work, for the solution of the nonlinear equations (11)-(13) we use fixed-point type methods. Specifically for the solution of (11), (12) we use what is called "Gradient flow in H^{-1} inner product/Relaxed fixed-point method", a type of relaxed fixed-point that can be thought as the gradient flow of the corresponding parabolic equation. This method at every iteration is significantly cheaper than Newton or nonlinear multigrid solvers and its convergence was found to be robust. To speed up the convergence of the method we scale the pseudo-time using the technique in [44]. An optimal choice of pseudo-step size can be obtained by linear search methods (cf. [45]).

For the solution of the corresponding linearized algebraic systems arising from the numerical discretization of the equations we use sparse LU and sparse Cholesky solvers utilizing libraries from [46] or geometric linear multigrid [47], while taking advantage of the sparse symmetric positive-definite mass and stiffness matrices that have block structure due to the use of the symmetric interior penalty DG-FE variant.

6. Conclusion

We have devised a mathematical model describing biofilm growth and phagocytosis by neutrophils, incorporating virulence factors such as diffusing toxin and anaerobic metabolism. First, (a nonspatial) version of the model was analyzed via stability analysis to gain insight, then numerical simulations of the full spatial continuum model were performed to understand its behavior. We demonstrated the importance of the virulence factors for biofilm survival under neutrophil phagocytosis. Our various test in 1D and 2D showed that spatial distribution and distance from the diffusing oxygen source elicits different outcomes regarding the survival or elimination of the biofilm infection under neutrophil immune response. We explained some of those outcomes based on the insights we obtained doing the simple nonspatial stability analysis. Our tests showed a threshold biofilm concentration that can guarantee infection persistence if it

is reached. Also we observed that a well oxygenated tissue would not allow biofilm colonies to grow enough, due to enhanced neutrophil killing, in order to reach the threshold concentration that is needed to survive. Hence hypoxia and the various mechanisms biofilm employ that are triggered in response to it (e.g., secretion of toxins and anaerobic metabolism), were found by our model to be essential for the persistence and spread of a bacterial infection. Finally, we showed an example where two virulent biofilm colonies (unable to survive alone in absence of the other) survive in synergy, "protecting" each other from phagocytosis by neutrophils. The two colonies example gives an insight and a potential explanation on how multiple colonies in a hypoxic setting can overcome the host immune system response synergistically by using virulence factors and shielding each other, in order to grow and expand.

Ours tests highlight the importance of local oxygen concentration level to boost neutrophil effectiveness against bacterial infection and this motivates further investigation by experimentalist on how this can be achieved, possibly based on some of the insights that our theoretical mathematical model provides. Also our phenomenological results might corroborate the need for therapies that increase oxygen levels on the infection site, like hyperbaric therapy [48], as a means to boost the immune response, even before the administration of antibiotics, which tests already showed that their effectiveness is increased by higher oxygen levels [49, 50], but eventually bacteria might become resistant to them.

In this work we modeled the effects of neutrophils without explicitly modeling their population or spatial evolution. In future work a model that can incorporate the neutrophils as discrete agents using techniques found in [51] utilizing a hybrid discrete continuous setting, could allow us more freedom to test different interactions, for example the use of NETs by neutrophils. Furthermore, the use of a phase field framework that will allow biofilm colonies to naturally expand spatially while incorporating cell-cell adhesion [52], could be more appropriate to be used in equation (2), within a hybrid discrete continuous framework mentioned above.

Acknowledgment

The author would like to thank Professors Philip S. Stewart and Isaac Klapper for comments and suggestions.

References

[1] L. Hall-Stoodley, J. W. Costerton, P. Stoodley, Bacterial biofilms: from the natural environment to infectious diseases, Nature Reviews Microbiology 2 (2) (2004) 95–108. doi:10.1038/nrmicro821.
URL https://doi.org/10.1038/nrmicro821

[2] W. G. Characklis, K. C. Marshall, Biofilms, Wiley, New York, 1990.

[3] K. Lewis, Riddle of biofilm resistance, Antimicrobial Agents and Chemotherapy 45 (4) (2001) 999–1007. arXiv:https://journals.asm.org/doi/pdf/10.1128/AAC.45.4.999-1007.2001, doi:10.1128/AAC.45.4.999-1007.2001.
URL https://journals.asm.org/doi/abs/10.1128/AAC.45.4.999-1007.2001

[4] W. M. Nauseef, N. Borregaard, Neutrophils at work, Nature Immunology 15 (7) (2014) 602–611. doi:10.1038/ni.2921.
URL https://doi.org/10.1038/ni.2921

[5] J. Hirschfeld, Dynamic interactions of neutrophils and biofilms, Journal of Oral Microbiology 6 (1) (2014) 26102, pMID: 25523872. arXiv:https://doi.org/10.3402/jom.v6.26102, doi:10.3402/jom.v6.26102.
URL https://doi.org/10.3402/jom.v6.26102

[6] S. S. Yoon, R. F. Hennigan, G. M. Hilliard, U. A. Ochsner, K. Parvatiyar, M. C. Kamani, H. L. Allen, T. R. DeKievit, P. R. Gardner, U. Schwab, J. J. Rowe, B. H. Iglewski, T. R. McDermott, R. P. Mason, D. J. Wozniak, R. E. Hancock, M. R. Parsek, T. L. Noah, R. C. Boucher, D. J. Hassett, Pseudomonas aeruginosa anaerobic respiration in biofilms: Relationships

to cystic fibrosis pathogenesis, Developmental Cell 3 (4) (2002) 593–603. doi:https://doi.org/10.1016/S1534-5807(02)00295-2.
URL https://www.sciencedirect.com/science/article/pii/S1534580702002952

[7] A. do Vale, D. Cabanes, S. Sousa, Bacterial toxins as pathogen weapons against phagocytes, Frontiers in Microbiology 7 (2016) 42. doi:10.3389/fmicb.2016.00042.
URL https://www.frontiersin.org/article/10.3389/fmicb.2016.00042

[8] N. H. Hajdamowicz, R. C. Hull, S. J. Foster, A. M. Condliffe, The impact of hypoxia on the host-pathogen interaction between neutrophils and staphylococcus aureus, International Journal of Molecular Sciences 20 (22) (2019). doi:10.3390/ijms20225561.
URL https://www.mdpi.com/1422-0067/20/22/5561

[9] M. Bhattacharya, E. T. M. Berends, R. Chan, E. Schwab, S. Roy, C. K. Sen, V. J. Torres, D. J. Wozniak, Staphylococcus aureus biofilms release leukocidins to elicit extracellular trap formation and evade neutrophil-mediated killing, Proceedings of the National Academy of Sciences 115 (28) (2018) 7416–7421. arXiv:https://www.pnas.org/content/115/28/7416.full.pdf, doi:10.1073/pnas.1721949115.
URL https://www.pnas.org/content/115/28/7416

[10] M. Bhattacharya, E. T. M. Berends, X. Zheng, P. J. Hill, R. Chan, V. J. Torres, D. J. Wozniak, Leukocidins and the nuclease nuc prevent neutrophil-mediated killing of staphylococcus aureus biofilms, Infection and Immunity 88 (10) (2020). arXiv:https://iai.asm.org/content/88/10/e00372-20.full.pdf, doi:10.1128/IAI.00372-20.
URL https://iai.asm.org/content/88/10/e00372-20

[11] A. I. Abdul Hamid, L. Nakusi, M. Givskov, Y.-T. Chang, C. Marquès, P. Gueirard, A mouse ear skin model to study the dynamics of innate im-

mune responses against Staphylococcus aureus biofilms, BMC Microbiology 20 (1) (2020) 22. doi:10.1186/s12866-019-1635-z.
URL https://bmcmicrobiol.biomedcentral.com/articles/10.1186/s12866-019-1635-z

[12] A. R. Sultan, T. Hoppenbrouwers, N. A. Lemmens-den Toom, S. V. Snijders, J. W. van Neck, A. Verbon, M. P. M. de Maat, W. J. B. van Wamel, During the early stages of staphylococcus aureus biofilm formation, induced neutrophil extracellular traps are degraded by autologous thermonuclease, Infection and Immunity 87 (12) (2019). arXiv:https://iai.asm.org/content/87/12/e00605-19.full.pdf, doi:10.1128/IAI.00605-19.
URL https://iai.asm.org/content/87/12/e00605-19

[13] A. Thanabalasuriar, B. N. V. Scott, M. Peiseler, M. E. Willson, Z. Zeng, P. Warrener, A. E. Keller, B. G. J. Surewaard, E. A. Dozier, J. T. Korhonen, L. I.-t. Cheng, M. Gadjeva, C. K. Stover, A. DiGiandomenico, P. Kubes, Neutrophil Extracellular Traps Confine Pseudomonas aeruginosa Ocular Biofilms and Restrict Brain Invasion, Cell Host & Microbe 25 (4) (2019) 526–536.e4. doi:10.1016/j.chom.2019.02.007.
URL https://linkinghub.elsevier.com/retrieve/pii/S1931312819301039

[14] Y. Wu, I. Klapper, P. S. Stewart, Hypoxia arising from concerted oxygen consumption by neutrophils and microorganisms in biofilms, Pathogens and Disease 76 (4), fty043 (Jun 2018). doi:10.1093/femspd/fty043.
URL https://doi.org/10.1093/femspd/fty043

[15] J. Monod, The growth of bacterial cultures, Annual Review of Microbiology 3 (1) (1949) 371–394. doi:10.1146/annurev.mi.03.100149.002103.
URL https://doi.org/10.1146/annurev.mi.03.100149.002103

[16] C. Matz, Biofilms as Refuge against Predation, in: S. Kjelleberg, M. Givskov (Eds.), The Biofilm Mode of Life: Mechanisms and Adaptations, Horizon Bioscience, Norfolk, UK, 2007, p. 195–213.

[17] F. Günther, G. H. Wabnitz, P. Stroh, B. Prior, U. Obst, Y. Samstag, C. Wagner, G. M. Hänsch, Host defence against staphylococcus aureus biofilms infection: Phagocytosis of biofilms by polymorphonuclear neutrophils (pmn), Molecular Immunology 46 (8) (2009) 1805–1813. doi:https://doi.org/10.1016/j.molimm.2009.01.020.
URL https://www.sciencedirect.com/science/article/pii/S016158900900042X

[18] A. D. Wilde, D. J. Snyder, N. E. Putnam, M. D. Valentino, N. D. Hammer, Z. R. Lonergan, S. A. Hinger, E. E. Aysanoa, C. Blanchard, P. M. Dunman, G. A. Wasserman, J. Chen, B. Shopsin, M. S. Gilmore, E. P. Skaar, J. E. Cassat, Bacterial hypoxic responses revealed as critical determinants of the host-pathogen outcome by TnSeq analysis of staphylococcus aureus invasive infection, PLoS Pathog. 11 (12) (2015) e1005341.

[19] J. W. Hall, J. Yang, H. Guo, Y. Ji, F. C. Fang, The staphylococcus aureus airsr two-component system mediates reactive oxygen species resistance via transcriptional regulation of staphyloxanthin production, Infection and Immunity 85 (2) (2017) e00838–16. arXiv:https://journals.asm.org/doi/pdf/10.1128/IAI.00838-16, doi:10.1128/IAI.00838-16.
URL https://journals.asm.org/doi/abs/10.1128/IAI.00838-16

[20] D. Balasubramanian, L. Harper, B. Shopsin, V. J. Torres, Staphylococcus aureus pathogenesis in diverse host environments, Pathogens and Disease 75 (1), ftx005 (01 2017). arXiv:https://academic.oup.com/femspd/article-pdf/75/1/ftx005/23880323/ftx005.pdf, doi:10.1093/femspd/ftx005.
URL https://doi.org/10.1093/femspd/ftx005

[21] I. Klapper, J. Dockery, Finger formation in biofilm layers, SIAM Journal of Applied Mathematics 62 (2002) 853–869. doi:10.1137/S0036139900371709.

[22] I. Klapper, J. Dockery, Mathematical description of microbial biofilms,

SIAM Review 52 (2) (2010) 221–265. arXiv:https://doi.org/10.1137/080739720, doi:10.1137/080739720.
URL https://doi.org/10.1137/080739720

[23] N. N. McGovern, A. S. Cowburn, L. Porter, S. R. Walmsley, C. Summers, A. A. R. Thompson, S. Anwar, L. C. Willcocks, M. K. B. Whyte, A. M. Condliffe, E. R. Chilvers, Hypoxia selectively inhibits respiratory burst activity and killing of staphylococcus aureus in human neutrophils, The Journal of Immunology 186 (1) (2011) 453–463. arXiv:https://www.jimmunol.org/content/186/1/453.full.pdf, doi:10.4049/jimmunol.1002213.
URL https://www.jimmunol.org/content/186/1/453

[24] I. C. Thaarup, A. K. S. Iversen, M. Lichtenberg, T. Bjarnsholt, T. H. Jakobsen, Biofilm survival strategies in chronic wounds, Microorganisms 10 (4) (2022). doi:10.3390/microorganisms10040775.
URL https://www.mdpi.com/2076-2607/10/4/775

[25] P. S. Stewart, Biophysics of biofilm infection, Pathogens and Disease 70 (3) (2014) 212–218. arXiv:https://academic.oup.com/femspd/article-pdf/70/3/212/17943145/70-3-212.pdf, doi:10.1111/2049-632X.12118.
URL https://doi.org/10.1111/2049-632X.12118

[26] T. Zhang, N. G. Cogan, Q. Wang, Phase field models for biofilms. i. theory and one-dimensional simulations, SIAM Journal on Applied Mathematics 69 (3) (2008) 641–669.
URL http://www.jstor.org/stable/40233637

[27] T. Zhang, N. G. Cogan, Q. Wang, Phase-field models for biofilms ii 2-d numerical simulations of biofilm-flow interaction, Communications in Computational Physics 4 (1) (2008) 72–101. doi:https://doi.org/.
URL http://global-sci.org/intro/article_detail/cicp/7782.html

[28] N. Cogan, Incorporating toxin hypothesis into a mathematical model of persister formation and dynamics, Journal of Theoretical Biology 248 (2) (2007) 340–349. doi:https://doi.org/10.1016/j.jtbi.2007.05.021.
URL https://www.sciencedirect.com/science/article/pii/S0022519307002639

[29] A. Aristotelous, I. Klapper, Y. Grabovsky, B. Pabst, B. Pitts, P. Stewart, Diffusive transport through a model host-biofilm system, Phys. Rev. E 92-2 (2015) 022703.

[30] A. Aristotelous, Y. Grabovsky, I. Klapper, Heterogeneity formation within biofilm systems, European Journal of Applied Mathematics 29 (6) (2018) 1020–1034. doi:10.1017/S0956792518000402.

[31] P. S. Stewart, Diffusion in biofilms, Journal of Bacteriology 185 (5) (2003) 1485–1491. arXiv:https://journals.asm.org/doi/pdf/10.1128/JB.185.5.1485-1491.2003, doi:10.1128/JB.185.5.1485-1491.2003.
URL https://journals.asm.org/doi/abs/10.1128/JB.185.5.1485-1491.2003

[32] C. Alvarez-Ortega, C. S. Harwood, Responses of pseudomonas aeruginosa to low oxygen indicate that growth in the cystic fibrosis lung is by aerobic respiration, Molecular Microbiology 65 (1) (2007) 153–165. arXiv:https://onlinelibrary.wiley.com/doi/pdf/10.1111/j.1365-2958.2007.05772.x, doi:https://doi.org/10.1111/j.1365-2958.2007.05772.x.
URL https://onlinelibrary.wiley.com/doi/abs/10.1111/j.1365-2958.2007.05772.x

[33] O. Couvert, M.-L. Divanac'h, A. Lochardet, D. Thuault, V. Huchet, Modelling the effect of oxygen concentration on bacterial growth rates, Food Microbiology 77 (2019) 21–25. doi:https://doi.org/10.1016/j.fm.2018.08.005.
URL https://www.sciencedirect.com/science/article/pii/S0740002018300881

[34] N. Rabin, Y. Zheng, C. Opoku-Temeng, Y. Du, E. Bonsu, H. O. Sintim, Biofilm formation mechanisms and targets for developing antibiofilm agents, Future Medicinal Chemistry 7 (4) (2015) 493–512, pMID: 25875875. arXiv:https://doi.org/10.4155/fmc.15.6, doi:10.4155/fmc.15.6.
URL https://doi.org/10.4155/fmc.15.6

[35] A. Sharma, K. B. Wood, Spatial segregation and cooperation in radially expanding microbial colonies under antibiotic stress, The ISME Journal 15 (10) (2021) 3019–3033. doi:10.1038/s41396-021-00982-2.
URL https://doi.org/10.1038/s41396-021-00982-2

[36] A. C. Aristotelous, O. A. Karakashian, S. M. Wise, Adaptive, second-order in time, primitive-variable discontinuous galerkin schemes for a cahn–hilliard equation with a mass source, IMA Journal of Numerical Analysis 35 (3) (2015) 1167–1198. doi:10.1093/imanum/dru035.
URL https://doi.org/10.1093/imanum/dru035

[37] J. L. Bona, V. A. Dougalis, O. A. Karakashian, W. R. McKinney, Fully discrete methods with grid refinement for the generalized Korteweg-de Vries equation., Proceedings of the workshop on viscous and numerical approximations of shock waves, N.C. State University (1990) 117–124.

[38] J. L. Bona, V. A. Dougalis, O. A. Karakashian, W. R. McKinney, Conservative high order schemes for the Generalized Korteweg-de Vries equation., Philos. Trans. Royal Soc. London, Ser. 351 (1995) 107–164.

[39] D. N. Arnold, F. Brezzi, B. Cockburn, L. D. Marini, Unified analysis of discontinuous Galerkin methods for elliptic problems, SIAM J. Numer. Anal. 39 (5) (2001/02) 1749–1779 (electronic).

[40] B. Riviére, Discontinuous Galerkin Methods for Solving Elliptic and Parabolic Equations, SIAM, Philadelphia, 2008.

[41] D. A. D. Pietro, A. Ern, Mathematical Aspects of Discontinuous Galerkin Methods, Springer-Verlag, Berlin Haidelberg, 2012.

[42] K. Vemaganti, Discontinuous galerkin methods for periodic boundary value problems, Numer. Methods Partial Differential Eq. 23 (2007) 587–596.

[43] A. C. Aristotelous, N. C. Papanicolaou, A Discontinuous Galerkin Method for Unsteady Two-dimensional Convective Flows, American Institute of Physics (AIP) Conference Proceedings 1773 (2016) 110002.

[44] C.-S. Liu, S. N. Atluri, A novel time integration method for solving a large system of non-linear algebraic equations, Computer Modeling in Engineering & Sciences 31 (2) (2008) 71–84. doi:10.3970/cmes.2008.031.071.
URL http://www.techscience.com/CMES/v31n2/25166

[45] J. Nocedal, S. Wright, Numerical Optimization, Springer, New York, NY, 1999.

[46] T. A. Davis, Direct Methods for Sparse Linear Systems, Society for Industrial and Applied Mathematics, 3600 University City Science Center, Philadelphia, PA, United States, 2006. arXiv:https://epubs.siam.org/doi/pdf/10.1137/1.9780898718881, doi:10.1137/1.9780898718881.
URL https://epubs.siam.org/doi/abs/10.1137/1.9780898718881

[47] J. Bramble, Multigrid Methods, Research Notes in Mathematics Series, Chapman and Hall/CRC, London, 1993.

[48] N. E. Sanford, J. E. Wilkinson, H. Nguyen, G. Diaz, R. Wolcott, Efficacy of hyperbaric oxygen therapy in bacterial biofilm eradication, Journal of Wound Care 27 (Sup1) (2018) S20–S28, pMID: 29334015. doi:10.12968/jowc.2018.27.Sup1.S20.
URL https://doi.org/10.12968/jowc.2018.27.Sup1.S20

[49] D. Hu, L. Zou, W. Yu, F. Jia, H. Han, K. Yao, Q. Jin, J. Ji, Relief of biofilm hypoxia using an oxygen nanocarrier: A new paradigm for enhanced antibiotic therapy, Advanced science 7 (12) (May 2020). doi:10.1002/advs.202000398.
URL https://doi.org/10.1002/advs.202000398

[50] P. Jensen, S. Møller, C. Lerche, C. Moser, T. Bjarnsholt, O. Ciofu, D. Faurholt-Jepsen, N. Høiby, M. Kolpen, Improving antibiotic treatment of bacterial biofilm by hyperbaric oxygen therapy: Not just hot air, Biofilm 1 (2019) 100008. doi:https://doi.org/10.1016/j.bioflm.2019.100008.

[51] A. C. Aristotelous, R. Durrett, Chemical evolutionary games, Theoretical Population Biology 93 (2014) 1–13.

[52] I. Klapper, J. Dockery, Role of cohesion in the material description of biofilms, Physical review E 74 (2006) 031902.